High-Speed All- Optical Time Division Multiplexed Node

Z. Ghassemlooy, Wai Pang Ng, and H. Le-Minh
Optical Communication Research Group, School of Computing,
Engineering and Information Sciences, Northumbria University,
Newcastle upon Tyne, UK

Abstract: In future high-speed self-routing photonic networks based on all-optical time division multiplexing (OTDM) it is highly desirable to carry out packet switching, clock recovery and demultplexing in the optical domain in order to avoid the bottleneck due to the optoelectronics conversion. In this paper we propose a self-routing OTDM node structure composed of an all-optical router and demultiplexers based on the symmetric Mach-Zehnder (SMZ) and chained symmetric Mach-Zehder (CSMZ) for high bit rate OTDM demultiplexing, respectively. The paper investigates both numerically and by means of simulation the noise and crosstalk characteristics of the both single channel and multiple channel demultiplexers and the bit error rate (BER) performance of the proposed OTDM node. For BER of 10-9 and the total bit rates of 100 and 200 Gbps the power penalty incurred are about 2 and 2.5 dB, respectively compared with 2.5 Gbps back-to-back (B-B) system.

Keywords: All-optical division multiplexing, All-optical router, Demultiplexers

1. INTRODUCTION

The ever-increasing aggregate demand of electrically based time division multiplexing systems would have coped with the steady growth rate of voice traffic. However, since 1990, the explosive growth of the Internet and other bandwidth demanding multimedia applications, has meant that long-haul telecommunication traffic has been increasingly dominated by data not voice traffic [1]. Such systems suffer from a bandwidth bottleneck due to speed limitations of the electronics currently at less that 40 Gbps. This bottleneck limits the maximum data rate to considerably less than the THz bandwidth offered by an optical fibre. All-optical technology is proposed as the only viable option and is expected to play an ever increasing role in future ultra-high speed links/networks. Packet switching systems based on the dense wavelength division multiplexing (DWDM) and OTDM or combination of both technologies are capable of fully realising the ultra-high speed optical networks as a means to overcome the bandwidth bottleneck imposed by electrical TDM [1, 2]. In DWDM, a number of different data channels are allocated to discrete optical wavelengths offering a data rate of > 160 Gbps using a large of number of wavelength over a single fibre link [3 – 6]. There are a number of problems associated with the WDM systems such as (i) performance being highly dependent on the nonlinearities associated with fibre (Stimulated Raman scattering, Four wave mixing, and Cross phase modulation), and (ii) relatively static optical paths, thus offering no fast switching with high performance within the network. In OTDM scheme, a data packet is generated by interleaving time-delayed ultra-short optical pulse carriers (at single wavelength) with each is modulated with data signal at the base rate. Nevertheless, simultaneous demultiplexing of multiple high-speed OTDM channels is a challenging task due to the increased number of channels and the complexity of optoelectronic and optical devices operating at high bit rate (≥ 100 Gbit/s) resulting in a need of a solution in the optical domain [7]. The all-optical solution provides a scalable, flexible high bandwidth on demand (in excess of a few hundred Gbit/s) platform to meet the future service demands of the network [8 – 11]. In addition, it offers self-routing and self-clocking capabilities and can operate at 2nd and 3rd transmission windows (1300 nm and 1500 nm) for both broadcast and switched based networks. OTDM can be used side-by-side with WDM to further increase the network capacity especially at the back bone.

2. Principle of OTDM

Figure 1 show the generic block diagram of an OTDM transmission system including the all-optical switching node, where N optical base-line data channels, each of capacity M Gbps are multiplexed to give an aggregate rate of N x M Gbps. Both multiplexing and demultiplexing could be implemented either passively or actively. The former is based around mono-mode fibre components that are simple and cost effective, whereas the latter uses active device, such as 2 x 1 elect optic sampling switches, semiconductor optical amplifiers, and integrated optics to carry out multiplexing and demultiplexing [12 – 14]. The light source is a laser with high stability producing ultra-short pulses (< 2 ps). Direct modulation of the laser source is possible but the preferred method is based on employing external modulation where the optical signal is gated by the electronic data. The combination of these techniques allows the time division multiplexed data to be encoded inside a sub-nanosecond time slot, which is subsequently interleaved into a frame format. Optical interleaving can be carried out at the bit level or at the packet level where blocks of bits are interleaved sequentially. Here we have adopted the former option.

A simple conceptual description of a bit interleaved multiplexer is shown in Fig. 2. It uses a number of different length optical fibre delay lines (FDL) to interleave the channels. The propagation delay of each FDL is chosen to position the optical channel in its corresponding time slot in relation to the aggregate OTDM signal. Prior to this each optical pulse train is modulated by the data stream. The output of the modulators and an un-delayed pulse train, labelled the framing signal, are combined using a star coupler, or combiner, to produce the high bit rate OTDM signal. As shown in Fig. 2, the framing pulse is incorporated for clock recovery purpose (for details see section 3.3).

An OTDM packet is composed of a clock bit, address bits and payload, and a packet guard band. Multiplexing of the clock signal (CS) with each packet can be carried out in a number of ways such as: space division multiplexing (SDM), WDM, orthogonal polarization, intensity division multiplexing and time division multiplexing [15]. In SDM, the optical clock signal and payload are carried on separate fibres. Although this scheme is the simplest to implement, it has two main drawbacks: (i) the time varying differential delay between the clock and data signals due to temperature variation, which may affect fibres unequally, and (ii) high installation cost. In WDM scheme, different wavelengths are allocated to CS and payload [16]. This technique is only practical for predetermined path lengths between nodes in single hop networks such as point-to-point links or broadcast-and-select star networks. In a non-deterministic optical path length for asynchronous packet switching scheme, the relative delay between the CS and payload will be stochastic. Orthogonally-polarized clock synchronization schemes are more suitable for small size networks [17], whereas in larger networks correct polarization maintenance throughout the network is rather difficult due to the fibre polarization mode dispersion and other non-linear effects. Although synchronization based on transmission of high intensity optical CS offers simplicity, maintaining the clock position and its intensity level over a long transmission span is a problem due to the impact of fibre non-linearities [18]. Multiplexing of the CS in time domain with the same intensity and wavelength as the data signal is the preferred option, which is adopted in this work.

In photonic networks at the intermediate nodes packets are optically dropped and/or inserted via an add/drop unit, see Fig. 1. At the receiving end the OTDM signal are demultiplexed to recover the individual base-line data channels.

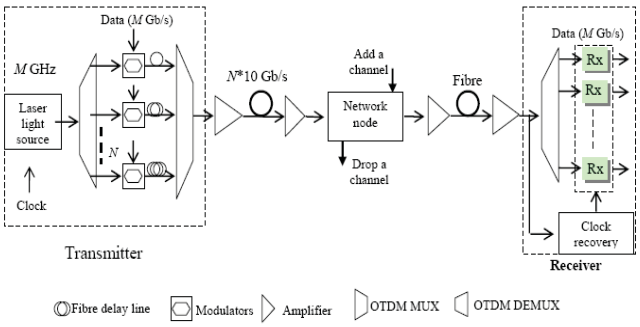

Fig.1: Block diagram of a typical OTDM transmission system.

2.1. OTDM Node

Figure 3 shows a block diagram of an OTDM switching node compose of two sections: a routing and channel add/drop module. The router is composed of clock and address bits extraction modules, a 1 × M optical switch, optical delay lines, and a number of optical amplifiers, whereas the add/drop module is composed of an SMZ demultiplexer and time slot multiplexer. At the add/drop module a particular channel within the switched OTDM packet is recovered by means of a single channel demultiplexer. At the node, the CS is extracted from the received OTDM packet using two inline SMZs which will be used as the CP for address extraction and demultiplexer modules. The extracted address bits are used as the CP in the 1 × M optical switch to route the entire delayed OTDM packet to one of its output ports. Detail operation of the router can be found in [19] and [20].

2.2. Demultiplexer

A number of optical configurations for OTDM demultiplexing have been proposed including the photonic serial-to-parallel converter (PSPC) based on the Lithium Niobate electro-opto modulator [21], surface-emitted second-harmonic generation (SESHG) employing hybridized semiconductor/silica waveguide circuits [22] and an array of optical single-channel SOA-based demultiplexers [23 – 25]. The SOA is the fundamental building block for the majority of optical switches because of its high extinction ratio, low cost and easy integration with other devices. Among these structures, the latter, based on the cross-phase modulation (XPM) in conjunction with interferometric configurations, is the most promising approach for current and future ultrahigh-capacity OTDM switching and demultiplexing because of its high extinction ratio, low cost and compact size, thermal stability, symmetrical SW profile, and low power operation [15][26][27]. The SOA-based demultiplexer includes different schemes such as terahertz optical asymmetric demuliplexer (TOAD) [23], ultrafast nonlinear interferometer (UNI) [24] and SMZ [25]. TOAD-based switches are composed of a short fibre loop and a nonlinear element (NLE) placed asymmetrically off the centre point of the loop [23]. Demultiplexing function is achieved solely by means of phase modulation. With the NLE being off-centred, an asymmetrical switching window (SW) profile is obtained due to the counter-propagating nature of the control pulse (CP) against the data pulse within the loop. These characteristics of the TOAD-based switches result in an increased crosstalk (CXT) and noise. The SW of the UNI is determined by the birefringence of the fibre used to separate the orthogonally-polarized components of the data pulses in time domain [28]. The main drawback of the UNI switch is its poor integrate-ability, since it requires at least 15 m of birefringent fibre to achieve the switching process [29]. Furthermore the switch needs to maintain and control the polarization to ensure reliability, which adds to the cost and complexity of the switch [30].

The SMZ structure provides the highest flexibility with a narrowest and symmetrical SW profile [19] [31]. Recently, for the first time, we reported an all-optical clock recovery module and a 1×2 OTDM router employing SMZs [19]. A 1× 2 router based on TOADs has been proposed for all-optical address recognition and single bit self-routing in a Banyan type network [32]. However, the orthogonally-polarized CP used in the router is rather difficult to maintain due to the polarization mode dispersion inherent in the optical fibre link. This problem can be avoided by using packets with signals that have identical polarization, intensity, pulse width and wavelength. In this paper we propose an all optical OTDM node structure composed of a router, a demultiplexer based on the SMZ, optical pre-amplifier and optical receiver. Here we propose and investigate single-channel and multi-channels demultiplexing based on SMZs. The former is relatively straightforward, whereas the later based on a chained SMZ configuration requiring only two-thirds of the number of SOAs compared with scheme

using an array of SMZ. Theoretical investigation of the BER performance of OTDM systems employing an all-optical demultiplexer and an optical receiver has been studied in [33] and [34]. Here we show an OTDM node structure where packet routing and channel demultiplexing is carried out in all-optical domain. Since practical evaluation of the BER performance of the proposed scheme requires complex and costly test bed, we have used a dedicated simulation package to carry out detailed simulation and evaluation of the proposed OTDM node. Predicted BER performance is compared with the simulation results, which in turn are assessed against a 2.5 Gbps B-B system.
The structure of this paper is as follows. The operation principles of the SMZ switch, CSMZ demultiplexer, the noise and crosstalk characteristics of the switch and the BER analysis are outlined in section 2. Simulation model and results are presented in Section 3. Finally, in Section 4, the concluding remarks are given.

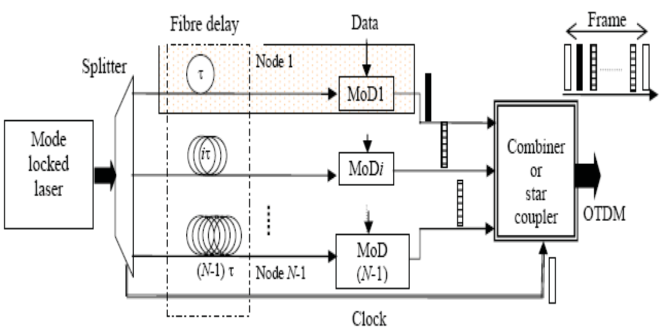

Fig. 2: A block diagram of bit interleaved OTDM

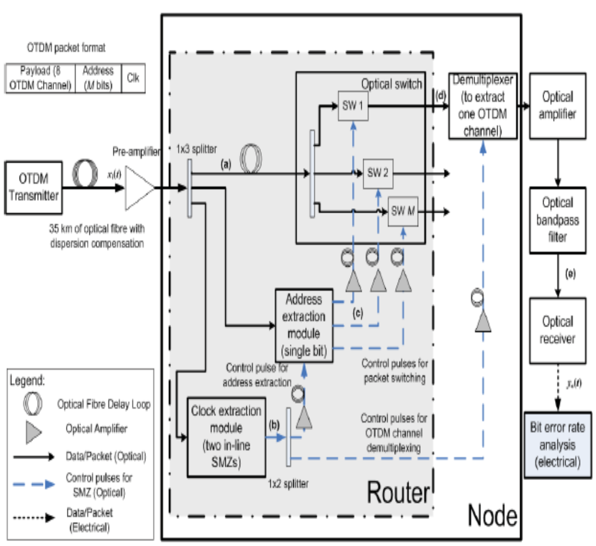

Fig.3: OTDM system block diagram with the proposed OTDM node

3. Theory

3.1. SMZ

A MZ configuration using two SOAs, one in each arm of the interferometer placed asymmetrically, and a number of 3-dB couplers are shown in Fig. 4. The operation principle is based on the optically induced refractive index change within the SOA when injected with the appropriately synchronised optical control signals that alter the phase conditions of data signals in the interferometer, thus resulting in switching. The induced non-linearity in the SOA is relatively long lived (hundreds of picoseconds) and therefore could be expected to limit the switching speed. Control and data signals, with orthogonal polarization, are fed into the switch via 3-dB couplers and co-propagate within the switch. In the absence of CPs, the data signals entering the switch via a coupler (C1) split into two equal intensity signals with 90o phase shift, E1(0) and E2(π/2), which propagate along the upper and lower arms of the interferometer, respectively. Couplers C2 and C3 are in the bar state for data signal therefore, introducing no additional phase shift Δϕ in the interferometer. With no CP present, E1 and E2 will experience the same relative Δϕ during propagation and recombine at the output of C4. The data signals at the output ports (O/P) 1 and 2 are given as:

$$E_{out,1} = E_{out}^{UA}(0) + E_{out}^{LA}(\pi) \qquad (1)$$

$$E_{out,2} = E_{out}^{UA}(\pi/2) + E_{out}^{LA}(\pi/2) \qquad (2)$$

where E_{out}^{UA} and E_{out}^{LA} are the signals at the output of the SOA in the upper and lower arms of the interferometer, respectively. Note that from (1), there is no signals emerging from the O/P1. However, with CPs present Δϕ is introduced between the two arms of the interferometer, thus causing the data signals to be switched to the O/P1, see Fig. 4. To achieve a complete switching at Δϕ = π, CP1 enters the interferometer via C2 just before the target data signal. The CP will then saturate SOA1, thus changing its gain as well as its phase characteristics. When the data signal enters the interferometer following the CP1, it will experience a different Δϕ (i.e. π) in the upper arm relative to the lower arm. The data signal emerging from the O/P1 is given as:

$$E_{out,1} = E_{out}^{UA}(\pi) + E_{out}^{LA}(\pi)\,. \qquad (3)$$

No signal will emerges from the O/P2 since E1 and E2 components will cancel each other, see Fig. 4(a).

Introducing the second CP2, delayed by Tdelay with respect to CP1, just after the data signal, into the interferometer via C3 will saturate SOA2, thus resulting in the same $\Delta\phi$ as in the upper arm, thereby resetting the switch. Therefore, with this mechanism the SMZ switch-on-and-off time is controlled by fast optical excitation process which overcomes the slow relaxation time. Note that Tdelay determines the SMZ nominal width of the SW. An optical polarization beam splitter (PBS) is used to separate the data and control signals at the output port of the SMZ. Practical switches and 3-dB couplers would normally have a small amount of net loss, which can be compensated by the gain of the SOAs. If necessary an additional amplifier could be incorporated at the output of the SMZ, but this will introduce additional noise.

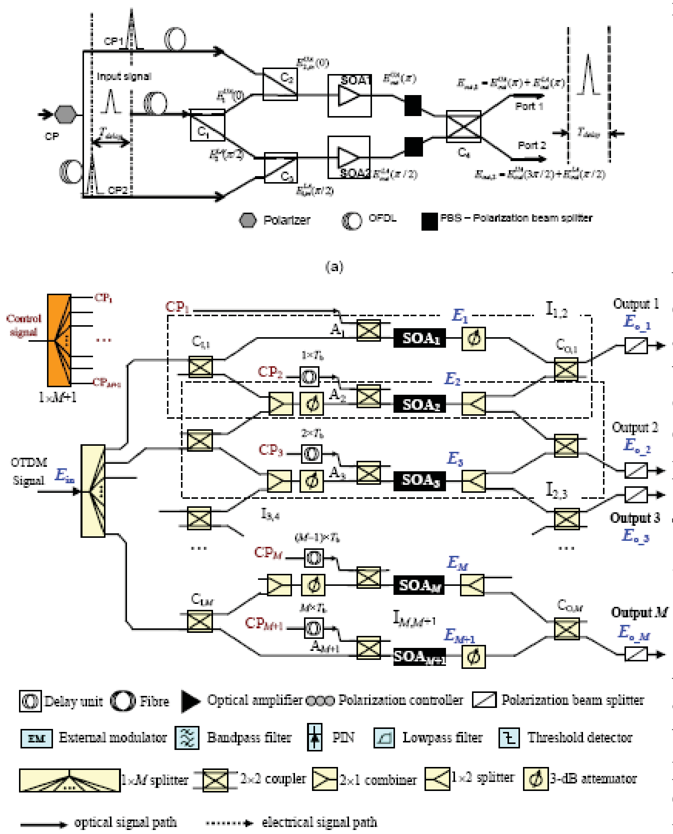

Fig.4: SMZ switch block diagram; (a) single channel, and (b) multi-channels

The electric fields at the O/P1 and O/P2 of the SMZ, in terms of the relative gain G and phase ϕ of the incident fields within the upper and lower arms can be expressed as:

$$\begin{pmatrix} E_{out,1}(t) \\ E_{out,2}(t) \end{pmatrix} = \begin{pmatrix} (1-\alpha)^{1/2} & j\alpha^{1/2} \\ j\alpha^{1/2} & (1-\alpha)^{1/2} \end{pmatrix} \begin{pmatrix} E^{UA}_{2,in}(t)G_1(t)e^{-j\phi} \\ E^{LA}_{1,in}(t)G_2(t)e^{-j\phi} \end{pmatrix} \quad (4)$$

where α is the coupling factor. For α of 0.5, $\left|E^{UA}_{1,in}(t)\right| = \left|E^{LA}_{1,in}(t)\right|$ and the relative phase difference is $\pi/2$, thus the signal powers at the output of the SMZ are given as:

$$P_{out,1}(t) = 0.125P_{in}(t)\cdot\left[G_1(t)+G_2(t)-2\sqrt{G_1(t)\cdot G_2(t)}\cos(\Delta\phi)\right] \quad (5)$$

$$P_{out,2}(t) = 0.125P_{in}(t)\cdot\left[G_1(t)+G_2(t)+2\sqrt{G_1(t)\cdot G_2(t)}\cos(\Delta\phi)\right] \quad (6)$$

where $\Delta\phi = -0.5\alpha_{LEF}\ln\left(G_1/G_2\right)$, αLEF is the linewidth enhancement factor, G1 and G2 are the temporal gain profiles of the SOAs1 and 2, respectively [35].

$$G_1(t) = \exp\left[\int_0^{L_{SOA}} \Gamma . g\left(z, t + \frac{z}{V_g}\right) dz\right] \quad (7)$$

$$G_2(t) = \exp\left[\int_0^{L_{SOA}} \Gamma . g\left(z, t + T_{delay} + \frac{z}{V_g}\right) dz\right] \quad (8)$$

where Γ is the confinement factor, g represents the differential gain of data and control pulses, t the time at which the temporal point of the data pulse enters the amplifier, Tdelay the temporal delay between the control pulses, z/Vg the time increment in the z direction, Vg is the group velocity of the control pulse and κ is the linewidth enhancement factor.

The SW is obtained by normalising (5) to Pin(t) as given in:

$$W_i(t) = 0.125\left[G_1(t)+G_2(t)-2\sqrt{G_1(t)G_2(t)}\cos\left(\Delta\phi\right)\right] \quad (9)$$

According to (9), the SMZ switch can provide an additional gain to the target signal, thus ensuring that the SW gain > 1. To solve (9) one needs to know precise value of αLEF and the gain profiles of the data signals at the output of the SOA1 and SOA2, respectively.

3.2. M-channel CSMZ

A M-channel CSMZ demultiplexer, Fig. 4(b), comprises of an 1 × M input splitter, a number of 3-dB 2 × 2 input CI,x and output CO,x couplers (x is channel number), 2 × 1 combiners, 1 × 2 splitters (see Table I) and identical SOAs in M + 1 CSMZ arms (A1 to AM+1). The inclusion of 3-dB attenuators located at each arm will ensure identical optical powers at the SOAs and CO,x couplers, thereby ensuring a balance state between each pair of adjacent arms. Thus, in the absence of a CP, no input signal emerges at the CSMZ output ports. For demultiplexing purposes, the extracted clock signal is split to M + 1 high-powered CPs with equal intensities. CP1 is applied to SOA1, just prior to the arrival of the data channel 1 to the interferometer I1,2, for setting I1,2 to a imbalance state where SOA1 and SOA2 will have different gain and phase profiles, thus demultiplexing the data channel 1 to the output 1. Since all other interferometers Ik,k+1 are still in the balance state, there should be no signal emerging from the other outputs. CP2 (delayed by 1 x Tb) is applied to SOA2 resulting in two simultaneous effects: (i) restoration of a balance state in I1,2 and (ii) creation of an imbalance state in I2,3 because of the gain and phase difference between SOA2 and SOA3. Thus, demultiplexing the data channel 2 to the CSMZ output 2. Similarly, demultiplexing of the remaining channels is carried out by applying the delayed CPs to the appropriate SOAs with delay by (x–1)×Tb to demultiplex the corresponding xth channel. Note that to complete demultiplexing of Mth channel, CPM+1 is applied to AM+1 to restore the balance state in IM,M+1.

Assume that the electrical field of the input signal is Ein [36], the fields at M-CSMZ output ports are determined by:

$$
\begin{aligned}
E_{o\_1} &= 0.5E_{in}M^{-0.5}\left[K_{1,1}g_1e^{-j\phi_1} - K_{1,2}g_2e^{-j\phi_2}\right]\\
E_{o\_m} &= 0.5E_{in}M^{-0.5}\left[K_{m,1}g_{m+1}e^{-j\phi_{m+1}} - K_{m,2}g_me^{-j\phi_m}\right]\\
E_{o\_m+1} &= 0.5E_{in}M^{-0.5}\left[K_{m+1,1}g_{m+1}e^{-j\phi_{m+1}} - K_{m+1,2}g_{m+2}e^{-j\phi_{m+2}}\right]\\
E_{o\_M} &= 0.5E_{in}M^{-0.5}\left[K_{M,1}g_{M+1}e^{-j\phi_{M+1}} - K_{M,2}g_Me^{-j\phi_M}\right]
\end{aligned} \tag{10}
$$

where gk and phase ϕk are the field gain and phase, respectively, of a complex gain of SOAk induced on the electrical field of signal propagating through [36] (1 ≤ k ≤ M + 1). m is even and the coefficients Kij are computed by (11) where αI,x and αO,x are the coupling factors of the input CI,x and output CO,x couplers, respectively.

$$
\begin{aligned}
&K_{1,1} = (1-\alpha_{I,1})^{1/2}(1-\alpha_{O,1})^{1/2};\ K_{1,2} = \frac{1}{2}\left(\alpha_{I,1}^{1/2} + \alpha_{I,2}^{1/2}\right)\alpha_{O,1}^{1/2};\\
&K_{m,1} = \frac{1}{2}(1-\alpha_{O,m})^{1/2}\left[(1-\alpha_{I,m})^{1/2} + (1-\alpha_{I,m+1})^{1/2}\right]; K_{m,2} = \frac{1}{2}\alpha_{O,m}^{1/2}\left(\alpha_{I,m-1}^{1/2} + \alpha_{I,m}^{1/2}\right)\\
&K_{m+1,1} = \frac{1}{2}(1-\alpha_{O,m+1})^{1/2}\left[(1-\alpha_{I,m})^{1/2} + (1-\alpha_{I,m+1})^{1/2}\right]; K_{m+1,2} = \frac{1}{2}\alpha_{O,m+1}^{1/2}\left(\alpha_{I,m+1}^{1/2} + \alpha_{I,m+2}^{1/2}\right);\\
&K_{M,1} = (1-\alpha_{I,M})^{1/2}(1-\alpha_{O,M})^{1/2};\ K_{M,2} = \frac{1}{2}\alpha_{O,M}^{1/2}\left(\alpha_{I,M-1}^{1/2} + \alpha_{I,M}^{1/2}\right)
\end{aligned} \tag{11}
$$

The demultiplexing switching window gains are therefore computed by (12) with $DW_x = P_{o\_x}/P_{in} = \left(E_{o\_x}E_{o\_x}^*\right)/\left(E_{in}E_{in}^*\right)$ and the power gain G relates to g as $G = g^2$ [36].

$$
\begin{aligned}
DW_1 &= \frac{1}{4M}\left[K_{1,1}^2G_1 + K_{1,2}^2G_2 - 2K_{1,1}K_{1,2}\sqrt{G_1G_2}\cos\Delta\phi_{1,2}\right]\\
DW_{m+1} &= \frac{1}{4M}\left[K_{m+1,1}^2G_{m+1} + K_{m+1,2}^2G_{m+2} - 2K_{m+1,1}K_{m+1,2}\sqrt{G_{m+1}G_{m+2}}\cos\Delta\phi_{m+1,m+2}\right]\\
DW_m &= \frac{1}{4M}\left[K_{m,1}^2G_{m+1} + K_{m,2}^2G_m - 2K_{m,1}K_{m,2}\sqrt{G_mG_{m+1}}\cos\Delta\phi_{m,m+1}\right];\\
DW_M &= \frac{1}{4M}\left[K_{M,1}^2G_{M+1} + K_{M,2}^2G_M - 2K_{M,1}K_{M,2}\sqrt{G_MG_{M+1}}\cos\Delta\phi_{M,M+1}\right]\\
&\text{where } \Delta\phi_{i,j} = -0.5\alpha_{LEF}\ln\left(G_i/G_j\right)
\end{aligned}
$$

(12)

3.3. Bit error rate (BER)

3.3.1. Router and demultiplexer

The dropped channel (i.e. demultiplexed by SMZ) is amplified and band limited via an optical pre-amplifier and an optical band-pass filter respectively, before being processed by the optical receiver to recover the original 2.5 Gbps data stream. The receiver unit consists of an ideal PIN photodetector, an amplifier, a sixth order electrical low-pass Bessel filter, a sampler and a threshold level detector, see Fig. 3. The system model for the BER analysis is adapted from [33] and [34]. The main sources of the noise are the relative intensity noise (RIN), SOA spontaneous emission (ASE), and noises associated with the receiver. It is assumed that noise associated with the source is negligible. RIN is caused by the combination of the timing jitters (mainly introduced by the ASE noise of lumped optical amplifier) between the control and signal pulses and a non-square SW profile of the SMZ, thus resulting in the intensity fluctuation of target signals and in the switching power penalty. RIN is defined in terms of the variance V(τ) and the expected value E[w(τ)] of the target signal energy which is given as [32]:

$$
RIN(\tau) = \frac{V(\tau)}{E^2[w(\tau)]} \tag{13}
$$

A non-ideal SW with a finite extinction ratio (ER) will result in CXT. CXT is defined in terms of non-target channels and target channel powers Po-nt and Pot, respectively which is given by:

$$
CXT = 10\log_{10}\left[\frac{P_{o-nt}}{P_{o-t}} = \frac{\frac{1}{T_c}\int_{t_0+T_b/2}^{t_0+T_c-T_b/2} W(t)p_p(t-t_0)dt}{\frac{1}{T_c}\int_{t_0-T_b/2}^{t_0+T_b/2} W(t)p_p(t-t_0)dt}\right] \tag{14}
$$

where pp(t) is the periodic train of data signal, Tb is the data bit duration, t0 is the centre of the SW, and Tc is the CP period. One interesting characteristic of SMZ switch is that both data and control signals co-propagate within the switch, thus resulting in reduced residual CXT compared with the TOAD-based switches where a small XGM between the counter-propagating pulses results in residual CXT [31], [37]. With reference to Fig. 5, the normalized total output power Po of two cascading SMZ stages induced CXT is computed by:

$$P_o = P_i\left(1 + CXT_1\right)\left(1 + CXT_2\right) = P_i\left(1 + CXT_t\right) \quad (15)$$

where the total CXT defined in terms of the 1st and 2nd stages $\left(CXT_t = CXT_1 + CXT_2 + CXT_1 CXT_2\right)$, and Pi is the power at the input.

The mean photocurrents for mark Im, and space Is are given as [33], [34], [38]:

$$\begin{aligned}\bar{I}_{\mathrm{m}} &= K \times \left(2P_s\right) \times \left(1 + CXT_t\right) \\ \bar{I}_{\mathrm{s}} &= K \times \left(2P_s\right) \times \left(CXT_t\right)\end{aligned} \quad (16)$$

where $K = \eta_{\mathrm{amp2\text{-}in}} G_{\mathrm{amp2}} \eta_{\mathrm{amp2\text{-}out}} L_{of} R_p$, Rp is the responsivity of the photodetector, ηamp2-in and ηamp2-out are the input and output coupling efficiencies of pre-amplifier, respectively, Gamp2 is the pre-amplifier gain, Lof is the optical filter loss, and Ps is the average received power without CXT. Assuming that the probabilities of the transmitted mark and space are equally likely (i.e. 0.5), the average received power for mark is 2Ps.

With reference to Fig. 5, the system is composed of four cascading amplification stages, thus the total noise figure NFtot for all stages is given as [39]:

$$NF_{tot} = NF_{amp1} + \frac{NF_{SW}}{G_{amp1}} + \frac{NF_{demux}}{G_{amp1} G_{SW}} + \frac{NF_{amp2}}{G_{amp1} G_{SW} G_{demux}} \quad (17)$$

The average photo-current equivalent of ASE is given by [33], [34], [38]:

$$I_{ASE-tot} = 0.5\, NF_{tot}\, G_{tot} \eta_{amp2-out} q B_o L_{of} \quad (18)$$

where Gtot = Gamp1×GSW× Gdemux×Gamp2, Bo is the optical bandwidths and q is the electron charge.

The noise sources contributing to the deterioration of the signal are the RIN σ^2_{RIN} from the source and from the last SMZ (i.e. SMZ-demux because of its narrow SW compared to the SMZ of the switch within the router), the ASE of SOAs in SMZ and pre-amplifier σ^2_{amp} and the shot noise σ_s^2 and thermal noise σ_{th}^2 at the receiver $\sigma^2_{receiver,x}$, defined as [33], [34]:

$$\sigma^2_{RIN,m} = \overline{I_m^2} RIN_T B_e + \left(2P_s K\right)^2 RIN_{SMZ-demux} \quad (19)$$

$$\sigma^2_{RIN,s} = \overline{I_s^2} RIN_T B_e \quad (20)$$

$$\sigma^2_{amp,x} = \frac{4\overline{I}_x I_{ASE-tot} B_e}{B_o} + \frac{I^2_{ASE-tot}\left(2B_o - B_e\right) B_e}{B_o^2} \quad (21)$$

$$\sigma^2_{receiver,x} = 2q\left(\overline{I_x} + I_{ASE-tot}\right) B_e + \left(\frac{4kT_k}{R_L} + i_a^2\right) B_e \quad (22)$$

where RINT is the RIN of the transmitter. Here we only consider RIN contribution from the last SMZ stage, RINSMZ can be computed from [33] for a given value of RMSjitter. Be is the electrical bandwidth of the receiver, x represents mark or space, k is the Boltzman's constant, Tk is the temperature in Kelvin, RL is the load resistance of photodetector and ia2 is the power spectral density of the electrical amplifier input noise current.

In (21), 1st and 2nd terms are the variances of the signal-ASE beat noise σ^2_{S-ASE} and the ASE-ASE beat noise $\sigma^2_{ASE-ASE}$, respectively, whereas in (22) 1st, 3rd and 4th terms represent σ_s^2, σ_{th}^2, and the amplifier noise, respectively. All noise sources are considered to be uncorrelated. As Bo >> Be, the beat noise is considered with Gaussian approximation. The total variance of noises is given by:

$$\sigma^2_{t,x} = \sigma^2_{RIN,x} + \sigma^2_{amp,x} + \sigma^2_{receiver,x} \quad (23)$$

Adopting the same approach used in [33], [34], [38] the BER is given by:

$$BER = \frac{1}{2} erfc\left(\frac{Q}{\sqrt{2}}\right) \quad (24)$$

where

$$Q = \frac{\overline{I_m} - \overline{I_s}}{\sigma_{t,m} + \sigma_{t,s}} \quad (25)$$

Since the expressions for the switching windows for SMZ and CSMZ are the same as in (9) and (12), respectively for α = 0.5 in (11), then (23) applies to both single channel and multi-channels demultiplexing.

Fig. 5: Cascaded amplifying stages

4. Simulation Model and Results

The proposed system shown in Fig. 3 is simulated using the Virtual Photonic Inc. (VPI) package, as shown in Fig. 6. The OTDM transmitter is composed of a single continuous-wave laser source at the wavelength of 1550 nm, a number of M-Z external modulators (modulated at the base rate of 2.5 Gbps), and a number of fibre delay lines. The laser sources used at the OTDM node to generate OTDM packets have a 3 ps pulse width at the same wavelength of 1550 nm. The CP peak power depends on the size of the required SW at a particular SMZ. For the 1×M switch and demultiplexer modules the CPs have peak power of 215 and 90 mW, respectively. The CPs are passed through a 90o orthogonal polarizer to distinguish it from the 1 mW data pulse since both are at the same wavelength. OFDLs are used to provide the delay Tdelay between the two CPs at the input of the SMZ and time synchronisation between the control and data pulses. Simulation results for the BER performance is compared with the predicted data. Here we first investigate the characteristic of the SMZ, 1 x M OTDM router and demultiplexer followed by the system BER.

(i) SMZ switch: Two methods have been used to evaluate the SW of the SMZ: a numerical model (modified version of [40]), and a VPI simulation model (see Fig. 6). All the parameters used in the simulation are listed in Table I. The full wave at half maximum (FWHM) of pulses used is 3 ps which less than the transition time of the SOA with a length of 0.25 μm. For Tdelay of 10 ps the predicted switching gain profiles of data pulses, having propagated through the SOAs, are shown in Fig. 7. In the absence of CPs, a data pulse propagating through the SOAs experience an initial gain of 20.1 dB. The gain profile drop rapidly to a value of 2.8 dB after a high power and short duration CP is applied to saturate the SOAs. With identical gain profile, the SMZ SW profiles for a range of SW width (1-10 ps) are shown in the inset of Fig. 7.

Using (13) and (14) the SMZ RIN against the switching window width for different values of the RMSjitter are shown in Fig. 8(a). RIN increases with the RMSjitter particularly for narrower SW width. The maximum RIN values are approximately -24, -18 and -10 dB for RMSjitter values of 0.5, 1 and 2 ps, respectively. The RIN decreases as the SW width increases reaching a minimum value of ≈ -25.5 dB for almost all values of RMSjitter. Demultiplexing of non-target channels from the adjacent channels will occur unless the SW width is comparable to or smaller than the time slot of OTDM channels (but > FWHM of the pulse). Figure 8(b) shows CXT against the SW width (or Tdelay) for the SOA length of 0.25 mm for different OTDM data rates. Lowest CXT is observed at low data rate of 2.5 Gbps increasing with the data rate. For all data rates, CXT increases with the SW size reaching maximum values of 0 and -4 dB for 1oo and 200 Gbps data rate, respectively at SW width of 20 ps (a very wide SW compared to the data bit duration).

(ii) 1 x M OTDM router and demultiplexer: The OTDM packet having propagating through a long length of fibre and a number of SOAs, see Fig. 9(a), is split and fed into the clock, address extraction and the main switch (with dedicated delay) modules. The extracted CS with a high extinction ratio (ER) of 30 dB is shown in Fig. 9(b). Figure 9(c) depicts the extracted address bit stream used as the CP in 1 X M switch for forwarding the whole OTDM packet to the correct output port as illustrated in Fig. 9(d). From Fig. 9(d) the ER is about 50 dB compared with 24 dB for the input OTDM packet. 36 dB gain in the ER is due to low residual gain residing outside the SMZ SW (see Fig. 7). The recovered OTDM channel at output of the demultiplexer is outlined in Fig. 9(e) with the ER of 44 dB. The drop in the ER is due to the noise associated with the SOA within the demultiplexer.

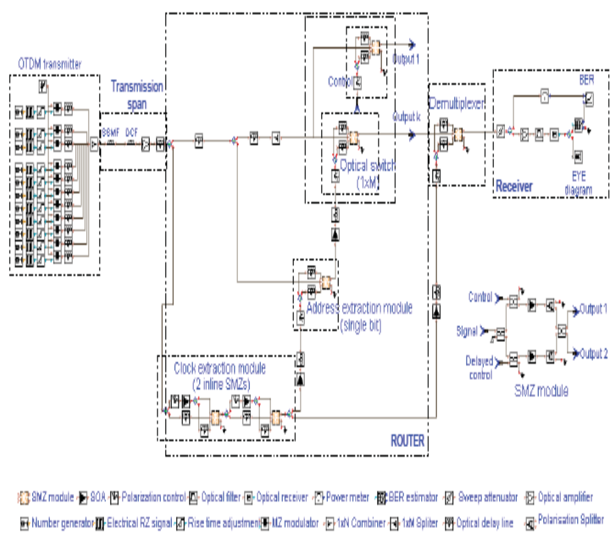

Fig. 6 : A schematic VPI® simulation model of 1×M OTDM system

4.1. BER Results

We have used theoretical and simulation methods to evaluate the BER performance of the OTDM node incorporating a router and a demultiplexer. In the simulation we evaluated the BER for return-to-zero (RZ) pseudo random binary sequence (PRBS) of length of 213 -1 and equal probability for mark and space. The base-band (B-B) bit rate is 2.5 Gbps with RZ pulse format to ensure that intersymbol interference induced by post-detection electrical filtering has negligible impact. All the receiver sensitivity measures are referred to an average BER of 10-9. All significant system parameters adopted from experimental work reported in [41], [42] and [43] are listed in Table 1. In VPI simulation, BER estimation is based on sampled signals with noise represented in noise bins by means of the global parameters. The noise bins bear the statistical information of the noise. Figure 10(a) shows the measured and simulated BER curves for the 2.5 Gbps B-B, 100 and 200 Gbps OTDM packets. The average received optical power Prx was measured for 2.5 Gbps B-B at the input of the optical receiver. For all measurements, it was ensured that the overall system gain is kept at 25 dB for the same optical receiver parameters. For high SOA gains the optical receiver sensitivity becomes dependent on the Bo and the signal-ASE and the ASE-ASE beat noises becomes dominant, and the.

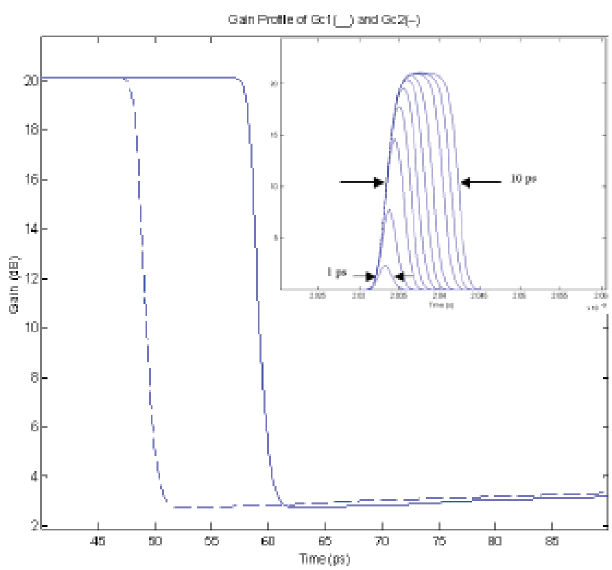

Fig. 7: Gain profile of the data signals in SMZ, and inset is the resulting switching window with width from 1ps to 10 ps

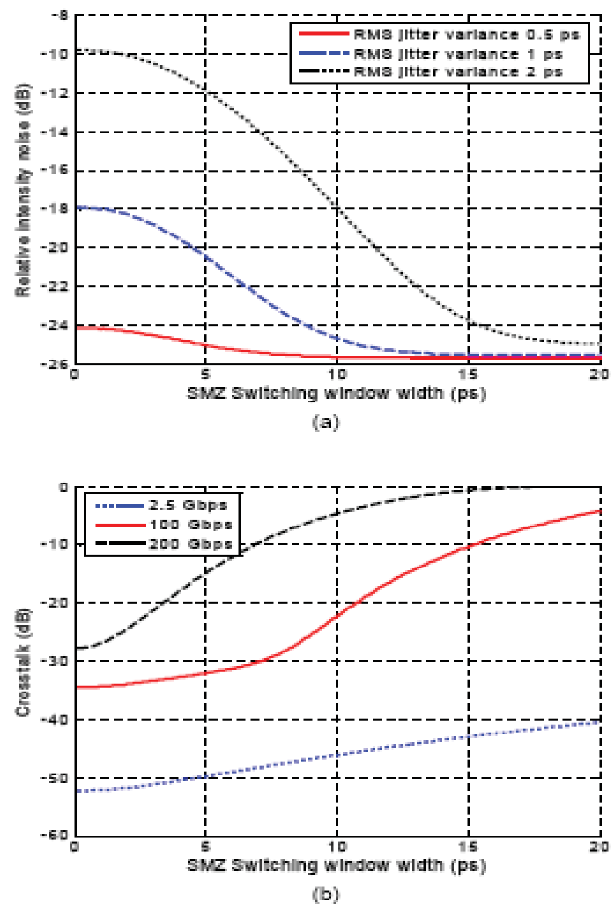

Fig.8: (a) Relative intensity noise against the switching window width for different values of RMSjitter and (b) channel crosstalk against the switching window width for different total bit rates

Table 1: Transfer function of coupler, combiner and spliter

	Schematic	Transfer function
2×2 coupler	E_{in_1}, E_{in_2} → 1-α, α → E_{o_1}, E_{o_2}	$\begin{bmatrix} E_{o\_1} \\ E_{o\_2} \end{bmatrix} = \begin{bmatrix} (1-\alpha)^{1/2} & j\alpha^{1/2} \\ j\alpha^{1/2} & (1-\alpha)^{1/2} \end{bmatrix} \begin{bmatrix} E_{in\_1} \\ E_{in\_2} \end{bmatrix}$
2×1 combiner	E_{in_1}, E_{in_2} → E_o	$E_o = \frac{1}{\sqrt{2}}(E_{in\_1} + E_{in\_2})$
1×*M* splitter	E_{in} → E_{o_1}, E_{o_2}, ⋮, E_{o_M}	$E_{o\_1} = E_{o\_2} = \ldots = E_{o\_M} \frac{E_{in}}{\sqrt{M}}$

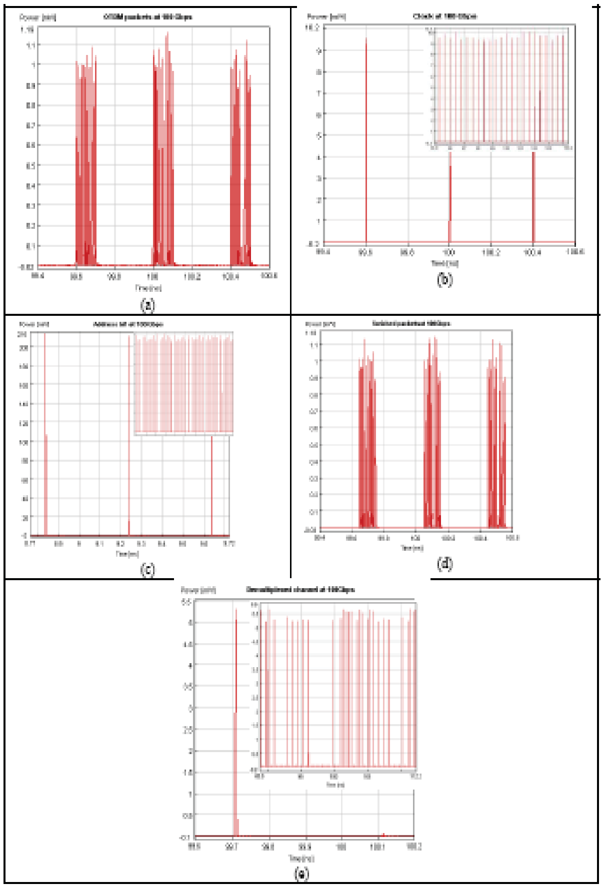

Fig. 9: Optical waveforms (a) input DM packet,(b) recovered clock pulses (inset clock bit stream), (c) address pulses (inset address bit stream), (d) switched OTDM packet and (e) demultiplexed channel (inset enlarged view)

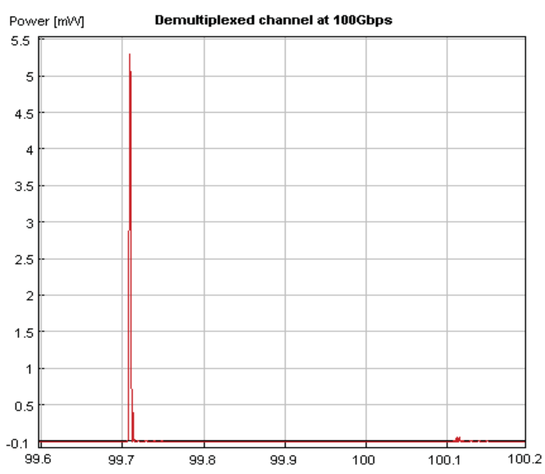

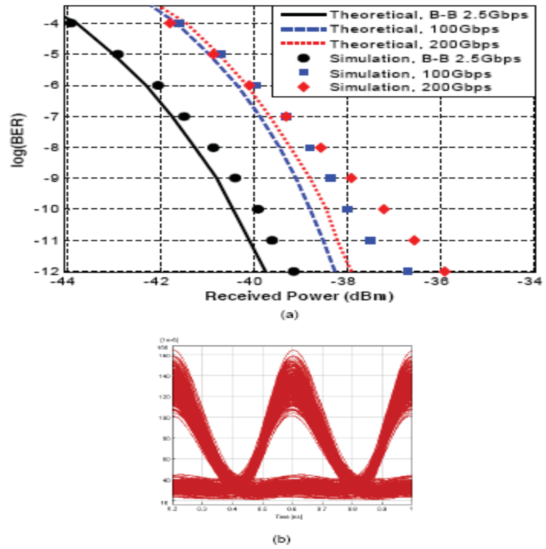

Fig. 10: Numerical and simulated BER for 2.5, 100 and 200 Gbps, and (b) the eye diagram for demultiplexed data channel at 2.5 Gbps and BER of 10-9

As shown in Fig. 10(a), for the 2.5 Gbps B-B without a router-demultiplexer, the calculated and simulated curves show good agreement, with only a small difference of < 0.4 dB at BER of 10-9. For 100 and 200 Gbps incorporating a router and a demultiplexer, the predicted BER curves display comparable characteristics, whereas the simulated curves are slightly worse with power penalties of 0.5 and 1 dB at BER of 10-9 for 100 and 200 Gbps, respectively. Compared with the B-B case, at BER of 10-9 the combined power penalties for the router and demultiplexer are about 2 and 2.5 dB for 100 and 200 Gbps, respectively. For BER < 10-9 the simulated power penalties increases by a few dB compared with predicted results. The most probable causes of the power penalties are mainly due to the RIN and ASE associated with SMZs and various insertion losses. Note that the SMZ switch with ER (> 30 dB) results in time-switching with ERs in excess of 50 dB, effectively eliminating CXT interference. An intersection of BER curves at BER of 10-4 and 10-5 is explained as follow. In VPI simulation model the BER estimation is based on the bit stream reference, thus providing more accurate results for low values of Q (i.e. BER > 10-4) in contrast to the predicted results. Finally, Fig. 10(b) shows the simulated eye diagrams at the output yo(t) of optical receiver for a single channel OTDM at BER of 10-9.

Figure 11(a) illustrates the time waveforms of 8 demultiplexed data channels using CSMZ at the receiving end of OTDM system described in Fig. 1.

Figure 11(b) shows the power penalties for different demultiplexed data channels, showing an average value of ~2 dB, which are similar to the obtained power penalty of the dropped channel by a single SMZ.

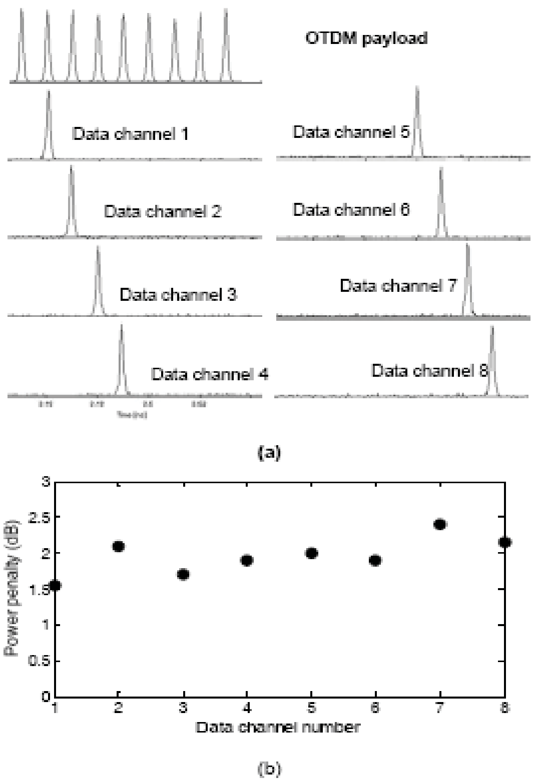

Fig.11: CSMZ demultiplexing of 8 channels OTDM packet's with 8 channels payload; (a) demultiplexed channels using CSMZ, and (b) the received power penalties at different data channels

5. Conclusions

We have proposed and simulated an OTDM node with an all-optical packet router employing a 1×M SMZ switch, and a CSMZ based demultiplexer for multiple-channel demultiplexing for high-speed (100-200 Gbps) optical network. Simulation results demonstrated that clock recovery, address recognition, packet routing and OTDM channel demultiplexing are possible with very little or no crosstalk at all. We investigated the BER performances numerically and by means of software simulation which showed good agreement. For BER of 10-9, the power penalty incurred are about 2 and 2.5 dB for 100 and 200 Gbps, respectively compared with 2.5 Gbps B-B case. The main contributors to power penalties were the RIN and ASE of the SMZs and SOAs, respectively for both single and multiple channels demultiplexing. The router proposed has a great potential for future ultra-high speed all-optical OTDM packet switched networks. CSMZ with shared SOA between two chained interferometer arms offered reduced complexity compared with the MZ based multiple-channel demultiplexers.

Table 2: System parameters

Parameter	Values
SOA	
Injection current	0.15 A
Length	0.25 mm
Active area	$2.4x10^{-13}m^2$
Transparent carrier density	$1.4x10^{24}m^{-3}$
Confinement factor	0.15
Differential gain	$2.78x10^{-20}m^2$
Linewidth enhancement	5.0
Recombination coeff. A	$1.43x10^8$ 1/s
Recombination coeff. B	$1.0x10^{-16}m^3/s$
Recombination coeff. C	$3.0x10^{-41}m^6/s$
Initial carrier density	$3.0x10^{24}m^{-3}$
Data and control signals	
Data bit rate per channel R_b	2.5 Gbit/s
FWHM width of clock, address and data signals	3 ps
Control and data wavelength	1550 nm
Data signal peak power	1 mW
Control signal peak power	90 mW for 4-8 ps and 185 mW for 120-160 ps switching window sizes
Rise and fall times	1 ps
$\eta_{amp2-in}$	0 dB
$\eta_{amp2-out}$	0 dB
Optical gain (overall) G_{tot}	25 dB
L_{of}	-8.97 dB
R_p	1 A/W
R_L	50 Ω
T_k	293 K
i_a^2	10 pA/Hz$^{1/2}$
Electrical bandwidth B_e	$0.7R_b$
Optical bandwidth B_o	125 GHz
RMS_{jitter}	1 ps
NF	6 dB
Optical fibre length and loss	30 km and 6dB
DCF length and loss	5.4km and 3dB
Optical 3dB 2×2 couplers splitting ratio α	50:50

References

[1] J. P. Ryan, R. H. Kent, 'WDM: North American deployment trends', IEEE Communications Magazine, Feb. 1998, pp. 40-44

[2] E. Lowe, 'Current European WDM deployment trends', IEEE Communications Magazine, Feb. 1998, pp. 46-50

[3] A J. P Jue, and G. Xiao, "An adaptive routing algorithm for wavelength-routed optical networks with a distributed control scheme", Proc. of Ninth IEEE International Conference on Computer Communications and Networks, pp. 192-197, 2000.

[4] C.D. Chen, I. Kim, O. Mizuharta, T.V. Nguyen, K. Ogawa, R.E. Tench, L.D. Tzeng and P.D. Yeats,

"0 Gbit/sx25 ch (1Tbit/s aggregate capacity) WDM transmission over 342km of fibre', Elec. Lett., 1999, 35 (8), pp. 648-649
[5] K. Struyve, N. Wauters, P. Falcao, P. Arijs, D. Colle, P. Demeester, and P. Lagasse, 'Application, design, and evolution of WDM in GTS's pan-European transport network', IEEE Communications Magazine, March 2000, pp.114-121
[6] B. Zhu, L. Leng, L.E. Nelson, Y. Qian, S. Stulz, C. Doerr, L. Stulz, S. Chandrasekar, S. Radic, D. Vengsarkar, Z. Chen, J. Park, K. Feder, H. Thiele, J. Bromage, et al, '3.08 Tb/s (77 × 42.7 Gb/s) transmission over 1200 km of non-zero dispersion-shifted fiber with 100-km spans using C- and L-band distributed Raman amplification', Conference on Optical Fiber Communication, Technical Digest Series, 2001, 54 (4), pp. PD23/1-PD23/3
[7] S. W. Seo, K.Bergman and P. R. Prucnal, "Transparent optical networks with time division multiplexing", J. LW Tech, 14 (5), pp1039-1051, 1996
[8] K. J. Blow, J. K. Lucek, and K. Smith, 'Optical switching', SPIE, Vol. 1983 (Optics as a Key to High Technology), 1993, pp. 480-484
[9] J. G. Zhang, 'Very-high-speed fibre optic networks for broadband communications', I.E.E. Electronics & Communication Engineering Journal, Dec.1996, pp. 257-267
[10] M. Nakazawa, T. Yamamoto, K. R. Tamura, '1.28Tbit/s-70km OTDM transmission using third- and fourth-order simultaneous dispersion compensation with a phase modulator', Electronics Letters, 2000, 36 (24), , pp. 2027-2029
[11] M. Nakazawa, T. Yamamoto, and K. R. Tamura M., "1.28Tb/s – 70km OTDM transmission using third and fourth order simultaneous dispersion compensation with a phase modulator", Proc ECOC 2000, Munich, Germany, Sept 2000, 2027-2029
[12] K. L. Deng et al, "Optical packet compressor for ultra-fast packet switching optical network", Electronics Letters, 33 (14), pp. 1237-1238, 1997
[13] H. Takara, I. Shake, K. Uchiyama, O. Kamatani, S. Kawanishi, and K. Sato, "Ultrahigh-speed optical TDM signal generator utilizing all-optical modulation and optical clock multiplication," in OFC/IOOC'98, Paper PD16
[14] F. Zamkotsian, K. Sato, H. Okamoto, K. Kishi, I. Kotaka, M. Yamamoto, Y. Kondo, H. Yasaka, Y. Yoshikuni, and K. Oe, "Generation and coding of a 100 Gbit/s signal by an InP-based optical multiplexer integrated with modulators," Electron. Lett., 1995, 31(7), pp. 578–579,
[15] P. Toliver, I. Glesk, and P.R. Prucnal, "All-optical clock and data separation technique for asynchronous packet-switched optical time-division-multiplexed networks," Opt. Commun., 2000, 173, pp. 101-106
[16] Y. Shimazu, M. Tsukada, "Ultrafast photonic ATM switch with output buffers," IEEE J. Lightwave Technol., 1992, 10, pp. 265-272
[17] I. Glesk, J. P. Solokoff, and P. R. Prucnal, "All-optical address recognition and self-routing in a 250 Gbit/s packet-switched network,", Electron. Lett., 1994, 30 (16), pp. 1322-1323
[18] K. L. Deng, I. Glesk, K. I. Kang, and P. R. Prucnal, "Unbalanced TOAD for optical data and clock separation in self-clocked transparent OTDM networks," IEEE Photon. Technol. Lett., 1997, 9, pp. 830-832
[19] R. Ngah, Z. Ghassemlooy, and G. Swift, "Simulation of an all optical time division multiplexing router employing symmetric Mach-Zehnder (SMZ)," Sep. 2002, HFPSC2002, pp. 130-136
[20] H. Le-Minh, Z., Ghassemlooy, and W. P. Ng, "A novel node architecture for all-optical packet switched network," Proce. of 10th European Conf. on Networks and Optical Communs., London, UK., July 2005, pp. 209-216
[21] M. L. Dennis, W. I. Kaechele, W. K. Burns, T. F. Carruthers, and I. N. Duling, "Photonic Serial-Parallel Conversion of High-Speed OTDM Data," IEEE Pho. Tech. Lett., 2000, 12, pp. 1561-1563
[22] T. G. Ulmer, M. C. Gross, K. M. Patel, J. T. Simmons, P. W. Juodawlkis, B. R. Washburn, W. S. Astar, A. J. SpringThorpe, R. P. Kenan, C. M. Verber, and S. E. Ralph, "160-Gb/s Optically Time-Division Multiplexed Link with All-Optical Demultiplexing," IEEE Light. Tech., 2000, 18, pp. 1964-1977
[23] J. P. Sokoloff, P. R. Prucnal, I. Glesk, and M. Kane, "A Terahertz optical asymmetric demultiplexer (TOAD)," IEEE Photon. Technol. Lett., 1993, 5, pp. 787-790,
[24] S. A. Hamilton, B. S. Robinson, T. E. Murphy, S. J. Savage, and E. P. Ippen, "100 Gbps optical time-division multiplexed network," IEEE Light. Tech., 2002, 20, pp. 2086-2100
[25] T. Tekin, C. Schubert, J. Berger, M. Schlak, B. Maul, W. Brinker, R. Molt, H. Ehlers, M. Gravert, and H.-P. Nolting, "160 Gbit/s error-free all-optical demultiplexing using monolithically integrated band gap shifted Mach-Zehnder interferometer (GS-MZI)," proc. IPR 2002, Vancouver, Canada, pp. IWC4, 2002
[26] R. P. Schreieck, M. H. Kwakernaak, and H. Melchior "All-optical switching at multi-100-Gb/s data rates with Mach-Zehnder interferometer

switches” IEEE J. Quantum Electron., 2002, 38 (8), pp. 1053-1061
[27] C. Schubert, J. Berger, S. Diez, H. J. Ehrke, R. Ludwig, U. Feiste, C. Schmidt, H. G. Weber, G. Toptchiyski, S. Randel, and K. Petermann, "Comparison of interferometric all-optical switches for demultiplexing applications in high-speed OTDM systems," IEEE Light. Tech., 2002, pp. 1-7
[28] K. L. Hall and B. S. Robinson, “Bit error characterization of 100 Gbit/s all-optical demultiplexers,” Proc. Conf. for Laser Electro Optic, Baltimore, MD, USA, 1999, pp. 214-215
[29] N. S. Patel, K. A. Rauschenbach, and K. L. Hall, “40 Gb/s demultiplexing using an ultrafast nonlinear interferometer (UNI),” IEEE Photon. Technol. Lett., 1996, 8, pp. 1695-1697
[30] P. R. Prucnal, R. J. Runser, and M. H. Singer “Optical switching techniques for the next generation Internet: a competitive study,” White Paper, Ultra Fast Optical Systems, 2000, pp. 1-14
[31] P. Toliver, R. J. Runser, I. Glesk, and P. R. Prucnal, “Comparison of three nonlinear optical switch geometries,” Proc. Con. Lasers and Electro-Optics, San Francisco, CA, 2000, pp. 254-255
[32] I. Glesk, K. I. Kang, and P. R. Prucnal, “Demonstration of ultrafast all-optical packet routing,” Electron. Lett., 1997, 33, pp. 794-795
[33] K. Uchiyama, T. Morioka, S. Kawanishi, H. Takara, and M. Saruwatari, “Signal-to-noise ratio analysis of 100 Gb/s demultiplexing using nonlinear optical loop mirror,” J. Lightwave Technol., 1007, 20 (2), pp. 618-624
[34] N. A. Olsson, “Lightwave systems with optical amplifiers,” J. Lightwave Technol., 1999, 7(7), pp. 1071-1082
[35] M. Eiselt, W. Pieper, and H. G. Weber, “SLALOM: semiconductor laser amplifier in a loop mirror,” J. Lightwave Technol., 1995, 13 (10), pp. 2099-2112
[36] M. Eiselt, W. Pieper, and H. G. Weber, "SLALOM: Semiconductor Laser Amplifier in a Loop Mirror," IEEE Light. Tech., 1995, 13, pp. 2099-2112
[37] C. Y. Cheung, Z. Ghassemlooy, G. Swift, and A. Decker, “Crosstalk and noise characteristics of non-linear optical loop mirror demultiplexer and terahertz optical asymmetric demultiplexer,” Proc. Inter. Sympo. On Commun. Sys., Networks and DSP, 2000, pp. 59-63
[38] G. P. Agrawal, “Fiber-optic Communication Systems,” 2nd Edition, 1997, J. Wiley, pp.163
[39] D. M. Baey, P. Gallion, and R. S. Tucker, “Theory and measurement techniques for the noise figure of optical amplifier,” Opt. Fib. Tech., 2000, 6, pp. 122-154
[40] G. Swift, Z. Ghassemlooy, A. K. Ray, and J. R. Travis, "Modelling of semiconductor laser amplifier for the terahertz optical asymmetric demultiplexer," IEE Proc.-Circuits Devices Syst., 1998, 145 (2), pp. 61-65
[41] H. G. Weber, R. Ludwig, U. Fieste, C. Schmidt, C. Schubert, J. Berger, E. Hilliger, M. kroh, T. Yamamoto, “High-speed all-optical signal processing in optical communication systems,” Proc. Conf. on Lasers and Electro Optics, Long Beach, USA, 2002, pp. 620-621
[42] M. Heid, S. L. Jansen, S. Splater, E. Meissner, W. Vogt, and H. Melchior, “160-Gbits/s demultiplexing to base rates of 10 and 40Gbits/s with a monolithically integrated SOA-Mach-Zehnder interferometer,” ECOC 02, Copenhagen, Denmark, 2002, Paper 8.4.3
[43] R. Hess M. Caraccia-Gross, W. Vogt, E. Gamper, P. A. Besse, M. Duelk, E. Gini, H. Melchior, B. Mikkelsen, M. Vaa, K. S. Jepsen, K .E. Stubkjaer, and S. Bouchoule, “All Optical Demultiplexing of 80 to 10Gb/s Signals with Monolithic Integrated High-Performance Mach-Zehnder Interferometer,” IEEE Photonics Technology Letts., 1998, 10 (1), pp. 165-167